Letter

Intrinsic Exciton-Phonon Coupling and Tuning in ZnTe Nanowires Probed by Resonant Raman Scattering

Yingyan Yi,[1,2] Jason K. Marmon,[3] Yuanping Chen,[4] Fan Zhang,[1] Tao Sheng,[5] Priyalal S. Wijewarnasuriya,[4] Haitao Zhang,[6] and Yong Zhang[1,3,*]

[1] *Department of Electrical and Computer Engineering, University of North Carolina at Charlotte, Charlotte, North Carolina 28223, USA*

[2] *School of Science, Wuhan University of Technology, Wuhan, Hubei 430070, China*

[3] *Nanoscale Science Graduate Program, University of North Carolina at Charlotte, Charlotte, North Carolina 28223, USA*

[4] *US Army Research Laboratory, Adelphi, Maryland 20783, USA*

[5] *Optical Science and Engineering Graduate Program, University of North Carolina at Charlotte, Charlotte, North Carolina 28223, USA*

[6] *Department of Mechanical Engineering and Engineering Science, University of North Carolina at Charlotte, Charlotte, North Carolina 28223, USA*

(Received 8 September 2019; revised manuscript received 25 October 2019; published 21 January 2020)

We show in ZnTe that the 2LO to 1LO resonant Raman intensity ratio, a measure of electron-phonon coupling (EPC), exhibits a much larger intrinsic value than that previously reported and minimal change from bulk to 30 nm nanowires. However, the ratio can be tuned extrinsically over one order in magnitude controllably either during or after growth, and thus, allows for the programing of EPC or quantum information in nanoscale devices. This work helps to understand a matter of controversy in the literature for more than three decades, regarding the EPC size dependence in nanostructures, and provides unambiguous experimental results for validating EPC theories with reduced dimensionality.

DOI: 10.1103/PhysRevApplied.13.011001

At the nanoscale, material properties, including electron–phonon coupling (EPC), are expected to change from their bulk values. However, the degree of change in EPC has been a topic with sustained controversy for over three decades. For instance, in the perhaps most studied system, CdSe, after the initial reports of a 20-fold decrease in nanocrystals (NCs) relative to that of the bulk [1,2], conflicting results on the NC size dependence of EPC were reported: very weak or size independence [3–5] and increasing with decreasing size [6,7]. Inconsistency in experimental results makes it challenging to validate different theoretical models [1,3,8,9] and impractical to develop applications.

Optical spectroscopy is often applied to probe EPC, where the intensity ratios of phonon replicas are typically used to extract the Huang-Rhys factor, S, that measures the EPC strength and is related to the relative lattice relaxation between the two states of an electronic transition [10]. Inconsistency between experimental approaches and conditions may partially explain the EPC controversy [11,12]. For instance, the S factors are predominately extracted from resonant Raman scattering (RRS) [1–3,5,6,13–15], but also from photoluminescence (PL) [16,17], PL excitation [18], and pump-probe measurements [11]. Excitation energy is another important variable, especially for RRS, even in bulk materials [6,9,15,19–21]. However, these considerations implicitly assume that the measured properties are intrinsic. Possible extrinsic effects associated with defects or impurities are either not considered or overlooked, although these extrinsic effects are shown to significantly affect EPC, even in bulk materials [19,22–24]. To answer the question to what extent EPC is affected by reducing dimensionality, we ought to know, first, the intrinsic bulk value; second, what is being measured in one specific experimental approach; and then what is the mechanism for the observed change.

Here, we show two different, but likely more significant, extrinsic sources that could contribute to the sustained controversy: defects and impurities in as-grown materials and defects induced unintentionally during measurements by the use of a high laser density. Our findings suggest that the literature controversy for nanostructures are mostly extrinsic and demonstrate the feasibility of controlling and tuning EPC in both bulk and nanostructures during and after growth. Furthermore, we point out that the theoretical models commonly adopted to extract the S factor from RRS are inapplicable to the problem. This

*yong.zhang@uncc.edu

work is of fundamental importance for developing comprehensive theories for understanding EPC across structural dimensions and material systems.

We focus on resolving the puzzling situation pertinent to the most widely used technique—RRS. In the literature, the so-called A''' term of Albrecht's RRS theory is often used to describe the Raman cross section of emitting n longitudinal optical (LO) phonons in the nanostructures [25]:

$$\sigma_R = |M^0_{e,g}|^4 \left| \sum_m \frac{\langle g,n|e,m\rangle\langle e,m|g,0\rangle}{E_{e,g} + m\hbar\omega_{LO} - \hbar\omega_0 + i\Gamma} \right|^2, \quad (1)$$

where $M^0_{e,g}$ is the dipole transition moment between the electronic ground state, $|g\rangle$, and dominant intermediate state, $|e\rangle$; $|g,n\rangle$ and $|e,m\rangle$ are, respectively, the vibrational states associated with $|e\rangle$ and $|g\rangle$; $\hbar\omega_0$ and $E_{e,g}$ are, respectively. the energy of the excitation photon and the intermediate state (e.g., the band gap, E_g); and Γ is the damping constant. Without lattice relaxation ($\langle g,n|e,m\rangle = \delta_{n,m}$), Eq. (1) describes Rayleigh scattering [25]. With lattice relaxation ($\langle g,n|e,m\rangle \neq \delta_{n,m}$), σ_R can, in principle, be related to S via the nonorthonormal product, $\langle g,n|e,m\rangle$. This formalism is widely used in size-dependence studies by relating the S factor to the intensity ratio of 2LO to 1LO Raman bands, $R_{21} = I_{2LO}/I_{1LO}$ [1,3,6,13,26–28]. Its applicability relies on theories that predict nonzero lattice relaxation via Fröhlich interactions, even for a bulk exciton [8,29,30].

For the most studied CdSe system, regardless of the trend of the size dependence, typically $R_{21} < 1$ or $<<1$ is found for CdSe NCs [12] and nanorods (NRs) [31,32], which would imply a small S factor, following Eq. (1). Similarly, $R_{21} < 1$ is reported for CdS NCs [33]. However, an early study on bulk CdSe showed practically no 1LO band, i.e., $R_{21} >> 10$ [34], which then suggests a huge S factor. Instead of assuming a large S and using Eq. (1), there the observation is attributed to the nearly forbidden 1LO scattering, when a 1s exciton state is involved as the intermediate state via Fröhlich interactions [19,35]. This explanation is based on a very different theory, where no simple correlation exists between S and R_{21}. Surprisingly, this alternative theory is largely ignored in EPC studies involving nanostructures, perhaps with one exception [9]. Interestingly, intentional surface roughing is found to enhance 1LO in bulk CdSe [34]. These findings should have indicated that it might not be appropriate to make the simple correlation between R_{21} and S.

ZnTe is ideal for exploring EPC due to its strong nLO RRS bands [36]. For bulk ZnTe, overall nLO RRS signals exhibit strong incoming resonance, when $\hbar\omega_0$ approaches E_g (2.254 eV) [20], whereas an individual mLO band is enhanced relative to nLO bands of $n \neq m$, when $\hbar\omega_0$ approaches $E_g + m\hbar\omega_{LO}$ (outgoing resonance) [21,23,36–38]. In general, $R_{21} >> 1$ is found under near-resonant excitation [20,21,23,37], unless $\hbar\omega_0$ is exactly $E_g + \hbar\omega_{LO}$, to yield 1LO enhancement. Similar to the case of CdSe [34], ZnTe 1LO also becomes invisible at low temperature [23]. However, some reports with excitation far away from $E_g + \hbar\omega_{LO}$ do yield $R_{21} \leq 1$ [36,38]. Therefore, major uncertainty exists, even for bulk ZnTe. It is unclear that the variation in R_{21} is due to that of the material or measurement, although it is indicated theoretically that impurities could reduce R_{21} [19,35].

For ZnTe NCs under 514.5 nm excitation, R_{21} is found to be reduced from about 2.7 to 0.3, when the size decreases from about 90 to 20 nm, and the changes are attributed to quantum size effects [14]. However, a similar trend, with comparable R_{21} amplitudes, is reported for ZnTe nanowires (NWs) with much larger dimensions, where quantum size effects would not apply [13]. Specifically, under 532 nm near-resonant excitation, when the NW diameter, d, is reduced from 200 to 90 nm, both R_{21} and S are reported to decrease monotonically from 1.3 to 0.7 and 1.8 to 1.0, respectively. Compared with the calculated bulk value of $S = 3.2$ using a widely adopted model [29], the reduction trend is explained to be due to reduced exciton polarization at the nanoscale [13], which is a frequently invoked reason used for other nanostructures.

Raman measurements are conducted at room temperature using a Horiba HR800 confocal Raman microscope, with a CCD detector and a 100× microscope lens (NA = 0.9). The spectral dispersion and spatial resolution are 0.44/pixel and about 0.36 μm, using a 532 nm laser. The spectrometer is calibrated to have a Si Raman band at 520.7 cm^{-1}, while a sufficiently low laser power (∼2–20 μW), about two orders lower than that reported in Ref. [13], is used to avoid laser-induced structural changes. The A_1 and E_{TO} modes of Te clusters at ∼120 and ∼140 cm^{-1} [39] emerge at about 200 μW for both bulk and NW samples, although the laser exposure times can vary significantly.

Before discussing the size effect of EPC, we first establish the intrinsic value for bulk ZnTe and investigate the effect of material imperfections. A set of bulk samples are studied: a high-quality crystal (B1) in bright reddish orange, and others (B2–B5) with varying defect concentrations in darker or gray colors. The defects in B2–B4 are likely to be O impurities [40], whereas B4 also contains about 2.5% Cd. A set of epitaxial thin-film (TF) samples, about 7–8 μm thick, grown by MBE on (211) Si substrates are also measured to investigate potential effects of the growth conditions. Each of these TF samples also has a thinner (∼150 nm), but highly defective, ZnTe layer grown unintentionally on the backside of the substrate. Over 40 ZnTe NWs, grown by CVD [41], are studied, either dispersed on SiO_2/Si substrates or TEM grids using isopropanol as the solvent. Their sizes are in the range of 30–800 nm, as measured by SEM. These NWs

are not expected to exhibit any significant quantum confinement effect, which prevents complications caused by inconsistent resonant conditions.

Figure 1 offers an overview of the typical RRS results obtained under the low excitation level for the three sample categories. Figure 1(a) includes representative PL and Raman spectra, while Fig. 1(b) shows their corresponding Raman spectra after removing the broad PL background. The representative R_{21} values are (evaluated using the integrated intensity and averaging over different spatial points) 10.5 ± 2.0 for B1, 2.0 ± 0.2 for B4, 7.5 ± 0.7 for TF1, and 6.9 ± 1.0 for a NW of $d \approx 84$ nm on a TEM grid. The results for all bulk and TF samples are summarized in Fig. 1(c). To exclude the possibility of major crystalline orientation dependence, B1 is also measured from a (110) cleave edge, which yields 7.7 ± 0.6, and thus, indicates that the orientation effect is minimal. However, defective bulk samples B2–B5 yield significantly reduced values, particular only 0.94 ± 0.05 for B5. The large fluctuation observed on B1 is due to two reasons: uncertainty in subtracting a strong PL background and the sensitivity of the Raman signal on the surface condition, because 1LO is largely forbidden [19,35]. It is interesting to note that, despite the TF samples containing a relatively high density of dislocation defects (with etch pit densities of 7.4×10^5–$2.8 \times 10^6/\text{cm}^2$), their R_{21} ratios are not affected significantly. Nevertheless, we do find that the thin ZnTe layer on the backside of the substrate exhibits much reduced R_{21} ratios (also very weak PL), as shown in Figs. 1(b) and 1(c) as "TF-B" for one of them, with its R_{21} ratio reduced to 0.59 ± 0.01. There

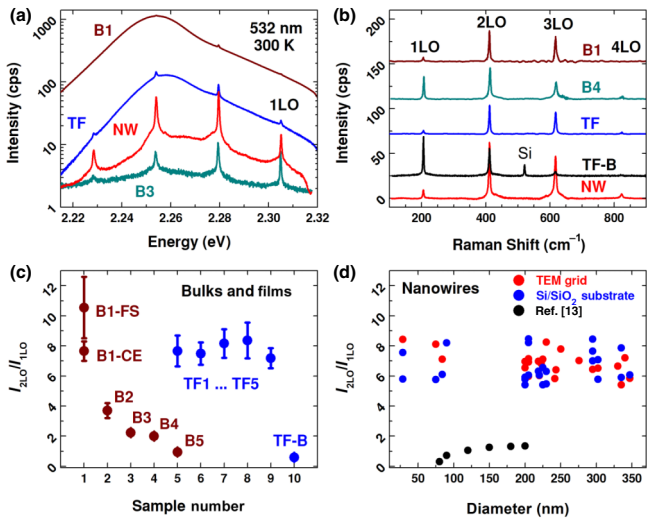

FIG. 1. Representative (a) photoluminescence and (b) resonant Raman spectra at low laser power. (c) R_{21} values for bulk ZnTe samples (wine) and ZnTe thin films (blue) and (d) for ZnTe nanowires supported by both a TEM grid (red) and SiO_2/Si substrate (gray).

is a general correlation between the crystalline quality and the R_{21} ratio: for instance, x-ray diffraction rocking curve line widths are 19″ for B1, around 160″ for TF samples, and around 1600″ for the TF-B samples. Also, along with the reduction in R_{21}, the intensity of the 3LO band also tends to reduce, relative to that of 2LO, as shown for B4 and TF-B in Fig. 1(b). Figure 1(d) displays the results for all investigated NWs, the diameters of which range from 29 to 350 nm. The average R_{21} among all NW samples is 7.1 ± 0.9, which is similar to those of TF samples, close to that of the bulk reference B1 and those of most previously reported bulk results [20,21,23,37], and thus, indicates that most of these NWs possess good crystalline quality. Importantly, our average NW value is roughly a factor of 23 larger than that of the smallest NW studied in Ref. [13], as compared in Fig. 1(d). We may conclude, at least down to around 30 nm in size, the R_{21} value or EPC exhibits little intrinsic size dependence in ZnTe NWs. The observed fluctuation is most likely to be due to variation in the surface conditions and crystallinity. Our results suggest that the previously reported size dependence of R_{21} for ZnTe nanostructures is likely to be extrinsic in nature. It is important to note that the reported ZnTe NW RRS spectra clearly show additional phonon modes related to Te clusters [13]; this hints that the excitation density is sufficiently high to induce structural changes that might affect the RRS results. This effect is very subtle because the laser damage threshold may vary by orders in magnitude for different materials and depend on other extrinsic factors (e.g., material dimensions and the supporting substrate) [42]. The absence of Te-related Raman bands in Fig. 1(b) indicates that the low excitation density employed here does not induce structural modification. The findings further suggest that reported results for other nanostructures in the literature should also be reexamined carefully.

The R_{21} ratio or EPC can be tuned by growth control, as demonstrated by the bulk samples B2–B5 and thin-film sample TF-B. Here, we show how the RRS signatures can be modified postgrowth by laser illumination in a controlled manner. We examine the changes in R_{21} and the appearance of the Te modes using two approaches: (1) under a fixed laser power with varying cumulative illumination time and (2) under a fixed illumination time with varying illumination power.

Figure 2 shows the results for one large and one small NW. For an 800 nm NW, first, it is illuminated by 750 μW for 5 s, then measured with 18 μW, repeating 18 times. Figures 2(a) and 2(b) depict a few typical Raman spectra and the relative changes in spectral features. Before illumination, there is a large R_{21} ratio of 8.3 and no observable Te Raman modes. Immediately after the first illumination, R_{21} is reduced to 6.5 and very weak Te modes at 124 and 142 cm^{-1} emerge. The intensity ratio of the 124 cm^{-1} Te mode to 2LO, $R_{\text{Te}} = I_{\text{Te}}/I_{2\text{LO}}$, changes relatively slowly until the 16th time, with R_{21} and R_{Te} reaching 5.1 and

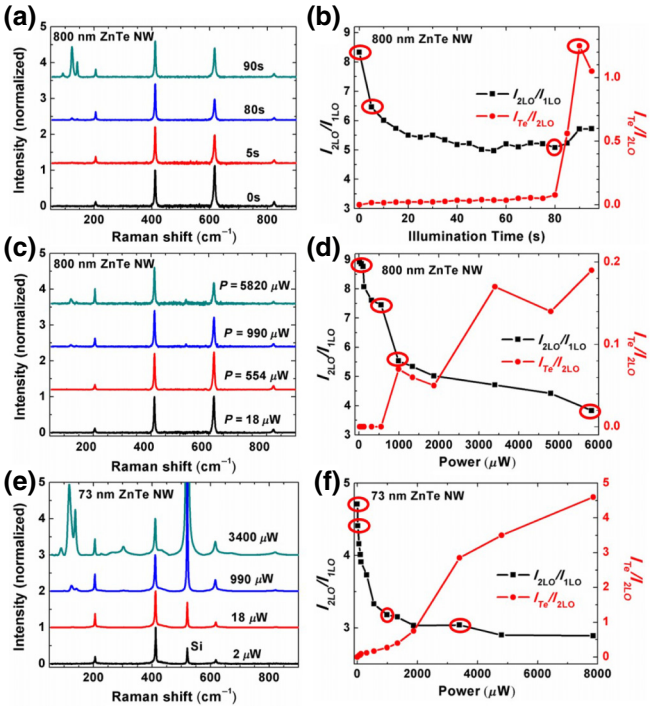

FIG. 2. Laser-induced modifications on Raman spectra of ZnTe NWs. (a),(b): a large NW subjected to repeated illumination of 750 μW/5 s, with (normalized) spectra in (a) for selected repeating windows, as marked on (b), and the ratios of I_{2LO}/I_{1LO} and I_{Te}/I_{2LO} at different repeating windows; (c),(d) for the same NW illuminated for 5 s under different powers; (e),(f) a small NW illuminated for 5 s under different powers.

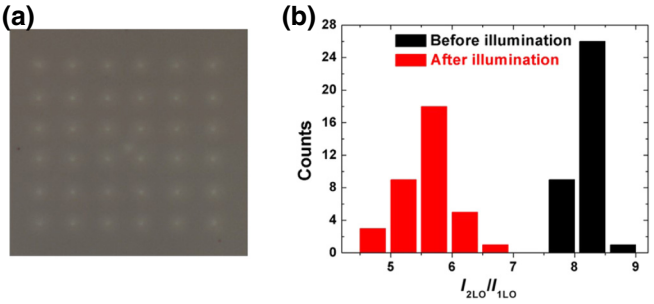

FIG. 3. A pattern of laser-induced modification: a 6×6 array with 5 μm spacing on a thin-film ZnTe. (a) Optical image showing illuminated locations. (b) A histogram plot of the R_{21} ratio before and after illumination.

0.08, respectively, but then the Te mode rises abruptly, with R_{Te} reaching 1.25. Second, it is illuminated with different powers up to 5.8 mW for 5 s each time. The results are shown in Figs. 2(c) and 2(d): R_{21} is reduced to 3.8 and R_{Te} increases to 0.2 after the highest power illumination. The results are combined effects of illumination power and time. We repeat the power-dependence measurements for a smaller NW of (73 ± 9) nm. The spectra shown in Fig. 2(e) confirm that there are no Te bands at low power with $R_{21} = 4.7$ (slightly defective), but the 1LO and Te modes are enhanced relative to that of 2LO with increasing power. R_{21} is reduced to 2.9 and R_{Te} increases to 4.6 after high-power illumination, as shown in Fig. 2(f). Although the appearance of Te modes is an indicator of structural change, the change could have already occurred, manifested as a change in R_{21}, before the Te modes actually become visible. Small NWs are more sensitive to the power, primarily because of lower thermal conductivity.

We further show that the level of modification is controllable, i.e., generating a R_{21} value in a prescribed range. A thin-film sample with a large initial R_{21} value is used. Figure 3 shows the results of an array of 36 points being illuminated with 4.8 mW for 20 s. Figure 3(a) is an optical image of the modified array, and the histogram plots of the R_{21} values before and after illumination are given in Fig. 3(b), with averages of 8.2 ± 0.2 versus 5.6 ± 0.5. They fall into two well-defined ranges. The results are stable, as a value of 4.7 ± 0.5 is remeasured 15 months later.

Because Huang-Rhys factor S is related to lattice relaxation between the two electronic transition states [10], lattice relaxation practically does not occur between two Bloch or extended states, such as a pair of valance and conduction band states, e.g., $<c\mathbf{k}|u_{\mathbf{q}}|c\mathbf{k}> - <v\mathbf{k}|u_{\mathbf{q}}|v\mathbf{k}> = 0$ [43]. For a free exciton, lattice relaxation is given by (using the excitonic wave functions [44])

$$\Delta_{ex}(\mathbf{q}) = \frac{1}{\omega_0^2} \sum_k |A_k|^2 (\langle ck|u_q|ck\rangle - \langle vk|u_q|vk\rangle), \quad (2)$$

where, for a large Wannier exciton, $A_{\mathbf{k}}$ will be the Fourier components of the exciton envelop function. Lattice relaxation, $\Delta_{ex}(\mathbf{q})$, will again practically be zero. Typically, it is only possible to relate S to the relative intensities of different phonon side bands in a straightforward manner for optical transitions, such as luminescence and absorption, involving a highly localized state [45] that exhibits a static lattice displacement between two charge states [46]. In a bulk crystal or a quantum-confined structure described by an envelope function, lattice vibrations induce only dynamic atomic displacements, but no change in their equilibrium positions. Direct calculations of lattice relaxation for nanostructures confirm this conclusion, with S values of about 10^{-3} or below [9,28]. Therefore, Eq. (1) is incapable of describing the intrinsic RRS of the bulk and nanostructures [47,48]. One would have to introduce some extrinsic effects to obtain a larger R_{21} or S factor, if insisting on using Eq. (1) [28], which, however, contradicts the fact that the highest quality bulk sample has the highest R_{21}. There are two basic theoretical frameworks representing two distinctively different approaches for treating EPC [45]: one including EPC in the vibrational states, e.g., Huang-Rhys theory [10], is more appropriate for highly localized states, while the other (e.g., as reviewed

by Permogorov [19]) includes EPC in the electronic states and is more appropriate for extended states. The alternative theory, treating the RRS as successively scattered LO phonons using discrete exciton bands as the intermediate states, is more appropriate for the problem [19]. Our results for the highest quality bulk ZnTe sample, B1, is in qualitative agreement with the latter theory, namely, 1LO scattering should be very weak (unless under the direct resonance condition [37]), but extremely sensitive to extrinsic perturbations.

Using ZnTe as a prototype system, we show no significant change in the intensity ratio, R_{21}, of RRS from bulk to nanostructures and, importantly, all have large R_{21} values of around 7–10. However, by controlling the impurity and/or defect level in bulk or thin-film ZnTe, we can reproduce practically the whole range of R_{21} variation reported in the literature for nanostructures of varying size. Our findings indicate that it is of paramount importance to prevent extrinsic effects in both materials and measurements for establishing the intrinsic reference. The basic assumption of nonzero lattice relaxation in bulk is inappropriate, and thus, the common practice of using the Albrecht A''' term to describe RRS is unjustified. The intensity ratios of the nLO RRS bands are related to EPC, but are also affected by various other processes, and thus, cannot be used for deriving the Huang-Rhys factor. This work provides a reliable experimental benchmark for validating theoretical methods.

The ability to control EPC during and after growth in the large window between the intrinsic value and achieved extrinsic value opens up opportunities for applications, such as in memory devices or sensing. For instance, both changes in nLO intensity distribution and relative intensity to the Te defect modes can be used for coding quantum information in the nanostructures for security and computing applications with preprogramed and reconfigured devices. The change in nLO ratios by surface modification with chemicals could lead to sensing applications.

ACKNOWLEDGMENTS

The work at UNC-Charlotte is supported by ARO/Electronics (Grant No. W911NF-16-1-0263). Y.Y. acknowledges support from the China Scholarship Council for his visit to UNCC, and Y.Z. acknowledges support from a Bissell Distinguished Professorship at UNCC. We thank Nimtech for providing the high-quality ZnTe crystal.

[1] A. P. Alivisatos, T. D. Harris, P. J. Carroll, M. L. Steigerwald, and L. E. Brus, Electron-vibration coupling in semiconductor clusters studied by resonant Raman spectroscopy, J. Chem. Phys. **90**, 3463 (1989).

[2] A. P. Alivisatos, A. L. Harris, N. J. Levinos, M. L. Steigerwald, and L. E. Brus, Electronic states of semiconductor clusters: Homogeneous and inhomogeneous broadening of the optical spectrum, J. Chem. Phys. **89**, 4001 (1988).

[3] M. C. Klein, F. Hache, D. Ricard, and C. Flytzanis, Size dependence of electron-phonon coupling in semiconductor nanospheres: The case of CdSe, Phys. Rev. B **42**, 11123 (1990).

[4] T. A. Nguyen, S. Mackowski, H. E. Jackson, L. M. Smith, J. Wrobel, K. Fronc, G. Karczewski, J. Kossut, M. Dobrowolska, J. K. Furdyna, and W. Heiss, Resonant spectroscopy of II-VI self-assembled quantum dots: Excited states and exciton-longitudinal optical phonon coupling, Phys. Rev. B **70**, 125306 (2004).

[5] V. M. Dzhagan, M. Y. Valakh, A. E. Raevskaya, A. L. Stroyuk, S. Y. Kuchmiy, and D. R. T. Zahn, Size effects on Raman spectra of small CdSe nanoparticles in polymer films, Nanotechnology **19**, 305707 (2008).

[6] G. Scamarcio, V. Spagnolo, G. Ventruti, M. Lugara, and G. C. Righini, Size dependence of electron-LO-phonon coupling in semiconductor nanocrystals, Phys. Rev. B **53**, 10489 (1996).

[7] J. C. Marini, B. Stebe, and E. Kartheuser, Exciton-phonon interaction in CdSe and CuCl polar semiconductor nanospheres, Phys. Rev. B **50**, 14302 (1994).

[8] S. Nomura and T. Kobayashi, Exciton–LO-phonon couplings in spherical semiconductor microcrystallites, Phys. Rev. B **45**, 1305 (1992).

[9] R. Rodríguez-Suárez, E. Menéndez-Proupin, C. Trallero-Giner, and M. Cardona, Multiphonon resonant Raman scattering in nanocrystals, Phys. Rev. B **62**, 11006 (2000).

[10] K. Huang and A. Rhys, Theory of light absorption and nonradiative transitions in F-centers, Proc. R. Soc. Lond. A: Math. Phys. Sci. **204**, 406 (1950).

[11] D. M. Sagar, R. R. Cooney, S. L. Sewall, E. A. Dias, M. M. Barsan, I. S. Butler, and P. Kambhampati, Size dependent, state-resolved studies of exciton-phonon couplings in strongly confined semiconductor quantum dots, Phys. Rev. B **77**, 235321 (2008).

[12] A. M. Kelley, Electron-phonon coupling in CdSe nanocrystals, J. Phys. Chem. Lett. **1**, 1296 (2010).

[13] Q. Zhang, J. Zhang, M. I. B. Utama, B. Peng, M. de la Mata, J. Arbiol, and Q. Xiong, Exciton-phonon coupling in individual ZnTe nanorods studied by resonant Raman spectroscopy, Phys. Rev. B **85**, 085418 (2012).

[14] S. Hayashi, H. Sanda, M. Agata, and K. Yamamoto, Resonant Raman scattering from ZnTe microcrystals - evidence for quantum size effects, Phys. Rev. B **40**, 5544 (1989).

[15] M. Brewster, O. Schimek, S. Reich, and S. Gradečak, Exciton-phonon coupling in individual GaAs nanowires studied using resonant Raman spectroscopy, Phys. Rev. B **80**, 201314 (2009).

[16] R. Heitz, I. Mukhametzhanov, O. Stier, A. Madhukar, and D. Bimberg, Enhanced Polar Exciton-LO-Phonon Interaction in Quantum Dots, Phys. Rev. Lett. **83**, 4654 (1999).

[17] S. A. Empedocles, R. Neuhauser, K. Shimizu, and M. G. Bawendi, Photoluminescence from single semiconductor nanostructures, Adv. Mater. **11**, 1243 (1999).

[18] E. Groeneveld, C. Delerue, G. Allan, Y. M. Niquet, and C. D. Donega, Size dependence of the exciton transitions in colloidal CdTe quantum dots, J. Phys. Chem. C **116**, 23160 (2012).
[19] S. Permogorov, in *Excitons*, edited by E. I. Rashba, M. D. Struge (North Holland Publishing Company, New York, 1982), pp. 177.
[20] R. L. Schmidt, B. D. McCombe, and M. Cardona, Resonant first- and second-order Raman scattering in ZnTe, Phys. Rev. B **11**, 746 (1975).
[21] M. Kwietniak, Y. Oka, and T. Kushida, Temperature dependence of Raman scattering and exciton luminescence spectra in ZnTe, J. Phys. Soc. Jpn. **44**, 558 (1978).
[22] P. H. Tan, Z. Y. Xu, X. D. Luo, W. K. Ge, Y. Zhang, A. Mascarenhas, H. P. Xin, and C. W. Tu, Resonant Raman scattering with the E+ band in a dilute GaAs1-xNx alloy (x=0.1%), Appl. Phys. Lett. **89**, 101912 (2006).
[23] A. A. Klochikhin, Y. V. Morozenko, and S. A. Permogorov, Resonance secondary radiation from ZnTe crystals, Sov. Phys. Solid State **20**, 1057 (1978).
[24] M. Balkanski, Effects of electron-phonon interaction in luminescence and light scattering, J. Lumin. **24/25**, 381 (1981).
[25] A. C. Albrecht, On the theory of Raman intensities, J. Chem. Phys. **34**, 1476 (1961).
[26] A. M. Kelley, Resonance Raman overtone intensities and electron–phonon coupling strengths in semiconductor nanocrystals, J. Phys. Chem. A **117**, 6143 (2013).
[27] A. V. Baranov, S. Yamauchi, and Y. Masumoto, Exciton–LO-phonon interaction in CuCl spherical quantum dots studied by resonant hyper-Raman spectroscopy, Phys. Rev. B **56**, 10332 (1997).
[28] T. D. Krauss and F. W. Wise, Raman-scattering study of exciton-phonon coupling in PbS nanocrystals, Phys. Rev. B **55**, 9860 (1997).
[29] R. Merlin, G. Güntherodt, R. Humphreys, M. Cardona, R. Suryanarayanan, and F. Holtzberg, Multiphonon processes in YbS, Phys. Rev. B **17**, 4951 (1978).
[30] S. Schmitt-Rink, D. A. B. Miller, and D. S. Chemla, Theory of the linear and nonlinear optical properties of semiconductor microcrystallites, Phys. Rev. B **35**, 8113 (1987).
[31] H. Lange, M. Mohr, M. Artemyev, U. Woggon, T. Niermann, and C. Thomsen, Optical phonons in colloidal CdSe nanorods, Phys. Status Solidi B: Basic Solid State Phys. **247**, 2488 (2010).
[32] H. Lange, M. Artemyev, U. Woggon, T. Niermann, and C. Thomsen, Experimental investigation of exciton-LO-phonon couplings in CdSe/ZnS core/shell nanorods, Phys. Rev. B **77**, 193303 (2008).
[33] J. J. Shiang, S. H. Risbud, and A. P. Alivisatos, Resonance Raman studies of the ground and lowest electronic excited state in CdS nanocrystals, J. Chem. Phys. **98**, 8432 (1993).
[34] E. Gross, S. Permogorov, Y. Morozenko, and B. Kharlamov, Hot-exciton luminescence in CdSe crystals, Phys. Status Solidi B **59**, 551 (1973).
[35] A. A. Gogolin and E. I. Rashba, Mechanism of strong resonant 1LO Raman scattering, Solid State Commun. **19**, 1177 (1976).
[36] J. F. Scott, R. C. C. Leite, and T. C. Damen, Resonant Raman effect in semiconductors, Phys. Rev. **188**, 1285 (1969).
[37] T. Kushida, A. Kurita, and Y. Fujikawa, Studies of exciton-polariton dynamics by luminescence and Raman scattering in ZnTe, J. De Phys. **46**, 209 (1985).
[38] Z. C. Feng, S. Perkowitz, and P. Becla, Multiple phonon overtones in ZnTe, Solid State Commun. **78**, 1011 (1991).
[39] A. S. Pine and G. Dresselh, Raman spectra and lattice dynamics of tellurium, Phys. Rev. B: Solid State **4**, 356 (1971).
[40] Z. T. Kang, H. Menkara, B. K. Wagner, C. J. Summers, and V. Valdna, Synthesis and characterization of oxygen doped ZnTe for powder phosphor application, J. Mater. Res. **20**, 2510 (2005).
[41] J. J. Huson, T. Sheng, E. Ogle, and H. Zhang, Reaction intermediate-induced vapor–liquid–solid growth of silicon oxide nanowires, CrystEngComm **20**, 7256 (2018).
[42] Q. Chen, H. Liu, H.-S. Kim, Y. Liu, M. Yang, N. Yue, G. Ren, K. Zhu, S. Liu, N.-G. Park, and Y. Zhang, Multiple-Stage Structure Transformation of Organic-Inorganic Hybrid Perovskite CH3NH3PbI3, Phys. Rev. X **6**, 031042 (2016).
[43] B. K. Ridley, *Quantum Processes in Semiconductors* (Oxford Science Publications, Oxford, 1999).
[44] F. Bassani and G. P. Parravicini, *Electronic States and Optical Transitions in Solids* (Pergamon, Oxford, 1975), pp. 190.
[45] Y. Zhang, W. K. Ge, M. D. Sturge, J. S. Zheng, and B. X. Wu, Phonon side-band of excitons bound to isoelectronic impurities in semiconductors, Phys. Rev. B **47**, 6330 (1993).
[46] S. Z. Karazhanov, Y. Zhang, L. W. Wang, A. Mascarenhas, and S. Deb, Resonant defect states and strong lattice relaxation of oxygen vacancies in WO/sub 3, Phys. Rev. B **68**, 233204 (2003).
[47] M. Cardona, in *Light Scattering in Solids II*, edited by M. Cardona, G. Güntherodt (Springer, Berlin, Heidelberg, 1982), pp. 19.
[48] Y. Zhang, Applications of Huang–Rhys theory in semiconductor optical spectroscopy, J. Semiconductors **40**, 091102 (2019).